



## Three-dimensional two-pion source image from Pb + Pb collisions at $\sqrt{s_{NN}} = 17.3$ GeV: New constraints for source breakup dynamics

NA49 Collaboration

C. Alt<sup>i</sup>, T. Anticic<sup>w</sup>, B. Baatar<sup>h</sup>, D. Barna<sup>d</sup>, J. Bartke<sup>f</sup>, L. Betev<sup>j</sup>, H. Białkowska<sup>t</sup>, C. Blume<sup>i</sup>, B. Boimska<sup>t</sup>, M. Botje<sup>a</sup>, J. Bracinik<sup>c</sup>, P. Bunčić<sup>j</sup>, V. Cerny<sup>c</sup>, P. Christakoglou<sup>a</sup>, P. Chung<sup>s</sup>, O. Chvala<sup>n</sup>, J.G. Cramer<sup>p</sup>, P. Csató<sup>d</sup>, P. Dinkelaker<sup>i</sup>, V. Eckardt<sup>m</sup>, D. Flierl<sup>i</sup>, Z. Fodor<sup>d</sup>, P. Foka<sup>g</sup>, V. Friese<sup>g</sup>, J. Gál<sup>d</sup>, M. Gaździcki<sup>i,k</sup>, V. Genchev<sup>r</sup>, E. Gładysz<sup>f</sup>, K. Grebieszko<sup>v</sup>, S. Hegyi<sup>d</sup>, C. Höhne<sup>g</sup>, K. Kadija<sup>w</sup>, A. Karev<sup>m</sup>, S. Kniege<sup>i</sup>, V.I. Kolesnikov<sup>h</sup>, R. Korus<sup>k</sup>, M. Kowalski<sup>f</sup>, M. Kreps<sup>c</sup>, A. Laszlo<sup>d</sup>, R. Lacey<sup>s,\*</sup>, M. van Leeuwen<sup>a</sup>, P. Lévai<sup>d</sup>, L. Litov<sup>q</sup>, B. Lungwitz<sup>i</sup>, M. Makariev<sup>q</sup>, A.I. Malakhov<sup>h</sup>, M. Mateev<sup>q</sup>, G.L. Melkumov<sup>h</sup>, M. Mitrosvki<sup>i</sup>, J. Molnár<sup>d</sup>, St. Mrówczyński<sup>k</sup>, V. Nolic<sup>w</sup>, G. Pál<sup>d</sup>, A.D. Panagiotou<sup>b</sup>, D. Panayotov<sup>q</sup>, A. Petridis<sup>b,1</sup>, W. Peryt<sup>v</sup>, M. Pikna<sup>c</sup>, J. Pluta<sup>v</sup>, D. Prindle<sup>p</sup>, F. Pühlhofer<sup>l</sup>, R. Renfordt<sup>i</sup>, C. Roland<sup>e</sup>, G. Roland<sup>e</sup>, M. Rybczyński<sup>k</sup>, A. Rybicki<sup>f</sup>, A. Sandoval<sup>g</sup>, N. Schmitz<sup>m</sup>, T. Schuster<sup>i</sup>, P. Seyboth<sup>m</sup>, F. Siklér<sup>d</sup>, B. Sitar<sup>c</sup>, E. Skrzypczak<sup>u</sup>, M. Slodkowski<sup>v</sup>, G. Stefanek<sup>k</sup>, R. Stock<sup>i</sup>, H. Ströbele<sup>i</sup>, T. Susa<sup>w</sup>, I. Szentpétery<sup>d</sup>, J. Sziklai<sup>d</sup>, M. Szuba<sup>v</sup>, P. Szymanski<sup>j,t</sup>, V. Trubnikov<sup>t</sup>, D. Varga<sup>d,j</sup>, M. Vassiliou<sup>b</sup>, G.I. Veres<sup>d,e</sup>, G. Vesztegombi<sup>d</sup>, D. Vranić<sup>g</sup>, Z. Włodarczyk<sup>k</sup>, A. Wojtaszek<sup>k</sup>, I.K. Yoo<sup>o</sup>, J.M. Alexander<sup>s</sup>, P. Danielewicz<sup>x,y</sup>, A. Kisiel<sup>v,z</sup>, S. Pratt<sup>y</sup>

<sup>a</sup> NIKHEF, Amsterdam, Netherlands

<sup>b</sup> Department of Physics, University of Athens, Athens, Greece

<sup>c</sup> Comenius University, Bratislava, Slovakia

<sup>d</sup> KFKI Research Institute for Particle and Nuclear Physics, Budapest, Hungary

<sup>e</sup> MIT, Cambridge, USA

<sup>f</sup> Henryk Niewodniczanski Institute of Nuclear Physics, Polish Academy of Sciences, Cracow, Poland

<sup>g</sup> Gesellschaft für Schwerionenforschung (GSI), Darmstadt, Germany

<sup>h</sup> Joint Institute for Nuclear Research, Dubna, Russia

<sup>i</sup> Fachbereich Physik der Universität, Frankfurt, Germany

<sup>j</sup> CERN, Geneva, Switzerland

<sup>k</sup> Institute of Physics Świętokrzyska Academy, Kielce, Poland

<sup>l</sup> Fachbereich Physik der Universität, Marburg, Germany

<sup>m</sup> Max-Planck-Institut für Physik, Munich, Germany

<sup>n</sup> Charles University, Faculty of Mathematics and Physics, Institute of Particle and Nuclear Physics, Prague, Czech Republic

<sup>o</sup> Department of Physics, Pusan National University, Pusan, Republic of Korea

<sup>p</sup> Nuclear Physics Laboratory, University of Washington, Seattle, WA, USA

<sup>q</sup> Atomic Physics Department, Sofia University St. Kliment Ohridski, Sofia, Bulgaria

<sup>r</sup> Institute for Nuclear Research and Nuclear Energy, Sofia, Bulgaria

<sup>s</sup> Department of Chemistry, SUNY Stony Brook, Stony Brook, NY, USA

<sup>t</sup> Institute for Nuclear Studies, Warsaw, Poland

<sup>u</sup> Institute for Experimental Physics, University of Warsaw, Warsaw, Poland

<sup>v</sup> Faculty of Physics, Warsaw University of Technology, Warsaw, Poland

<sup>w</sup> Rudjer Boskovic Institute, Zagreb, Croatia

<sup>x</sup> National Superconducting Cyclotron Laboratory, MSU, East Lansing, MI, USA

<sup>y</sup> Department of Physics and Astronomy, Michigan State University, East Lansing, MI, USA

<sup>z</sup> Department of Physics, The Ohio State University, Columbus, OH 43210, USA

\* Corresponding author.

E-mail address: Roy.Lacey@StonyBrook.edu (R. Lacey).

<sup>1</sup> Deceased.

## ARTICLE INFO

## Article history:

Received 30 July 2008

Received in revised form 3 September 2009

Accepted 13 January 2010

Available online 26 January 2010

Editor: V. Metag

## Keywords:

3D-imaging

HBT

Emission life time

## ABSTRACT

Source imaging methodology is used to provide a three-dimensional two-pion source function for mid-rapidity pion pairs with  $p_T < 70$  MeV/c in central (0–7%) Pb + Pb collisions at  $\sqrt{s_{NN}} = 17.3$  GeV. Prominent non-Gaussian tails are observed in the pion pair transverse momentum (outward) and in the beam (longitudinal) directions. Model calculations reproduce them with the assumption of Bjorken longitudinal boost invariance and transverse flow blast-wave dynamics; they also yield a proper time for breakup and emission duration for the pion source.

© 2010 Elsevier B.V. Open access under CC BY license.

Over the last several decades, the expansion dynamics and breakup lifetime for the exotic matter produced in relativistic heavy ion (RHI) collisions, have been of paramount interest [1,2]. Such enormous energy densities are created in the RHI collision zone, that de-confinement of nuclear matter is expected [3]. To gain an understanding of this state of matter, it is essential to study its dynamical evolution. The space–time extent of hot particle emission sources in heavy ion collisions has been studied for years via final-state correlations between two particles [4].

Years ago, pioneering work at the Alternating Gradient Synchrotron (AGS) [5] and by the NA49 Collaboration at the CERN Super Proton Synchrotron (SPS) [6], exploited the Hanbury-Brown–Twiss (HBT) correlations of hadron pairs in conjunction with fits to particle spectra, to estimate the dynamical properties of the reaction source in a blast wave model. The NA49 data for central Pb + Pb collisions at  $\sqrt{s_{NN}} = 17.3$  GeV indicated a strong longitudinal flow with an approximately boost invariant longitudinal velocity profile. These data also suggested a transverse expansion of the pion emission source with a duration of 8–9 fm/c. A more recent analysis [7] confirms these earlier findings while extending the beam energy dependence of the measurements to five separate SPS energies.

Several years ago, an alternative technique based on source imaging was introduced for model-independent extraction of emission sources in the pair-center-of-mass system (PCMS) [8–10]. This new methodology has provided a more faithful and detailed extraction of the actual 1D source function [11,12]. Recent theoretical developments [13–16] enable the extraction of three-dimensional (3D) profiles of the emission source.

This methodology, in both its 1D and 3D forms, has been employed for Au + Au reactions at  $\sqrt{s_{NN}} = 200$  GeV to obtain detailed information on both the spatial and the lifetime extents of the created emission source [12,17]. Here, we use the new methodology to again study reaction dynamics at the SPS but with identified pion correlations and extensively developed imaging techniques that explicitly include Coulomb effects and do not assume Gaussian sources. The resulting non-Gaussian source functions are interpreted in the context of a powerful new simulation model, THERMINATOR [18–20]. This approach explicitly includes all known resonance decays, longitudinal expansion, transverse expansion and a freeze-out hypersurface.

In this study, the source imaging technique is used to analyze NA49 Collaboration data for central (0–7%) Pb + Pb collisions at  $\sqrt{s_{NN}} = 17.3$  GeV, obtained at the SPS. Model comparisons allow tests of different aspects of the dynamics and, in particular, the extraction of the proper time for breakup and emission duration for the pion emission source. The picture that emerges has many similarities to that from the early work [6,7], but also adds interesting features and conclusions that preclude direct comparison.

The data presented here were taken by the NA49 Collaboration during the years 1996–2000. Lead beams of 158 A GeV from the CERN SPS accelerator were made incident on a lead foil of thickness 224 mg/cm<sup>2</sup>. Details of the experimental setup are discussed in Refs. [7] and [21]. Briefly, the NA49 Large Acceptance Hadron Detector achieves precision tracking and particle identification using four large Time Projection Chambers (TPCs). The first two of them are mounted in precisely mapped magnetic fields with total bending power of up to 9 Tm. Charged particles are detected by the tracks left in the TPCs and are identified by the energy deposited in the TPC gas. Mid-rapidity particle identification is further enhanced by a time-of-flight wall (resolution 60 ps). Charged particle momenta are determined from the deflection in the magnetic field. With the NA49 setup, a resolution of  $\delta p/p^2 \approx (0.3\text{--}7) \times 10^{-4}$  (GeV/c)<sup>-1</sup> is achieved. Event centrality is determined by a forward veto calorimeter which measures the energy of spectator matter. Approximately 3.9 million central events were analyzed.

The 3D correlation function,  $C(\mathbf{q})$ , and its 1D angle-averaged counterpart  $C(q)$ , were obtained as the ratio of pair to uncorrelated reference distributions in relative momentum  $\mathbf{q}$ , for  $\pi^+\pi^+$  and  $\pi^-\pi^-$  pairs. Here,  $\mathbf{q} = \frac{(\mathbf{p}_1 - \mathbf{p}_2)}{2}$  is half of the momentum difference between the two particles in the PCMS, and  $q$  is the modulus of the vector  $\mathbf{q}$ . The pair distribution was obtained by pairing particles from the same event; the uncorrelated distribution was obtained by pairing particles from different events. The Lorentz transformation of  $\mathbf{q}$  from the laboratory frame to the PCMS is made by a transformation to the longitudinally co-moving system (LCMS) frame along the beam direction followed by a transformation to the PCMS along the pair transverse momentum [22].  $C(q)$  is observed to be flat for  $50 < q < 100$  MeV/c and is normalized to unity over this range.

Mid-rapidity ( $|y_L - y_0| < 0.35$ , where  $y_L$  and  $y_0$  are particle and nucleus–nucleus centre-of-mass rapidities in the laboratory frame), low  $k_T$  ( $k_T < 70$  MeV/c, where  $k_T$  is half the transverse component of the pair total momentum)  $\pi^+\pi^+$  and  $\pi^-\pi^-$  pion pairs were selected for this study. Track merging and splitting effects were removed by appropriate cuts on both the pair and uncorrelated distributions. The merging cut required the two particles in a pair to be separated by at least 2.2 cm over 50 pad rows in the vertex TPCs [7]. A 20% increase in this minimum separation has resulted only in changes within the statistical errors. Similar evaluations for the other cuts indicate an overall systematic uncertainty which is comparable to or smaller than the statistical uncertainty.

The effects of track momentum resolution were assessed by jittering the momenta of the tracks in the data by the maximum momentum resolution,  $\delta p/p^2 \approx 7 \times 10^{-4}$  (GeV/c)<sup>-1</sup>. The resulting re-computed 1D and 3D correlation functions, which incorporate twice the effect of the momentum resolution, were found to be consistent with those obtained without momentum smearing. The

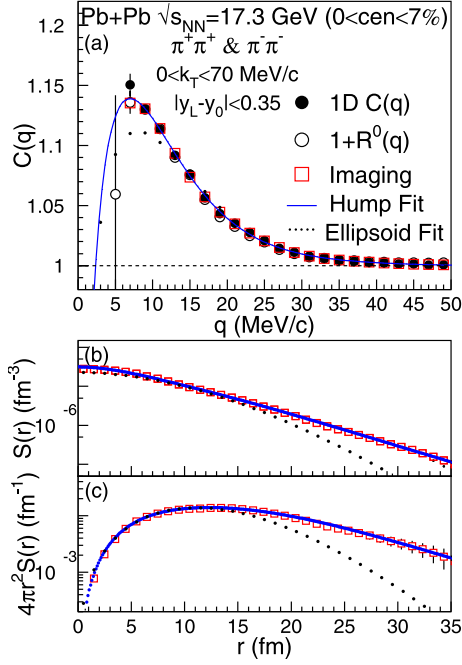


**Fig. 1.** (Color online.) Angle-averaged correlation function (a), source function (b) and radial probability density (c) for mid-rapidity pion pairs. Filled circles show correlation from direct averaging of the data. Error bars indicate statistical errors only; systematic uncertainties are smaller than statistical ones. Open circles represent correlation from fitting the data using angular decomposition. Squares show the imaged source and correlation corresponding to the imaged source. The dotted and solid lines represent, respectively, the fitted Gaussian and Hump Eq. (7) sources and their corresponding correlation functions.

correlation functions without additional smearing serve in the following as a basis for the extraction of source functions via imaging and fitting.

The imaging procedure employed uses the 1D imaging code of Brown and Danielewicz [8–10], which has been successfully used to image 1D correlation functions obtained at  $\sqrt{s_{NN}} = 200$  GeV [12]. Briefly, the technique numerically inverts the 1D Koonin–Pratt equation,

$$C(q) - 1 = R(q) = 4\pi \int dr r^2 K_0(q, r) S(r) \quad (1)$$

which relates the two-particle angle-averaged 1D correlation function,  $C(q)$ , to the 1D source function or image,  $S(r)$ . The latter gives the probability of emitting a pair of particles with a separation distance  $r$  in the PCMS. The 1D kernel  $K_0(q, r)$  incorporates the effects of Coulomb interaction and of Bose–Einstein symmetrization.

Contamination by uncorrelated pairs (weak decay products accepted by the track selection cuts, misidentified particles, etc.) dilute the correlation and reduce  $R(q)$ . It has been confirmed by simulation that the contamination is approximately constant in  $q$ , so that the reduction factor can be assumed to be  $q$ -independent. The source function  $S(r)$  then gets reduced by the same  $r$ -independent factor due to the linearity of Eq. (1).

Fig. 1(a) shows data points for the 1D correlation function in relation to the imaged source function in Figs. 1(b) and 1(c), for mid-rapidity, low  $p_T$  pion pairs. The source function indicates a tail for  $r \gtrsim 15$  fm which is qualitatively similar to that reported for RHIC data in Ref. [12]. As a check, the extracted source function is used as input to Eq. (1) to obtain a restored correlation function also shown in Fig. 1(a); excellent consistency is observed.

In parallel to the imaging procedure, two different functional forms were used to fit the measured correlation function directly,

as discussed below. The conclusion from the fits (see Fig. 1) is that a triaxial Gaussian, frequently termed ellipsoid, as used in traditional HBT methodology, poorly describes the correlation function at low  $q \gtrsim 13$  MeV/c (Fig. 1(a)), and this leads to a deviation from the tail of the imaged source function for large  $r \gtrsim 15$  fm (Fig. 1(b)). Fig. 1(c) highlights the fact that the tail for  $r \gtrsim 15$  fm contains a very significant fraction of the source. On the other hand, the Hump function (cf. Eq. (7) and discussion below) gives a good fit over a more extensive range.

For systematic access to the 3D source function  $S(\mathbf{r})$ , the 3D correlation function  $C(\mathbf{q})$  and source function  $S(\mathbf{r})$  were both expanded in a series with correlation moments  $R_{\alpha_1 \dots \alpha_l}^l(q)$  and source moments  $S_{\alpha_1 \dots \alpha_l}^l(r)$  in a Cartesian harmonic basis representation:

$$C(\mathbf{q}) - 1 = R(\mathbf{q}) = \sum_l \sum_{\alpha_1 \dots \alpha_l} R_{\alpha_1 \dots \alpha_l}^l(q) A_{\alpha_1 \dots \alpha_l}^l(\Omega_{\mathbf{q}}), \quad (2)$$

$$S(\mathbf{r}) = \sum_l \sum_{\alpha_1 \dots \alpha_l} S_{\alpha_1 \dots \alpha_l}^l(r) A_{\alpha_1 \dots \alpha_l}^l(\Omega_{\mathbf{r}}), \quad (3)$$

where  $l = 0, 1, 2, \dots$ ,  $\alpha_i = x, y$  or  $z$ ,  $A_{\alpha_1 \dots \alpha_l}^l(\Omega_{\mathbf{q}})$  are Cartesian harmonic basis elements ( $\Omega_{\mathbf{q}}$  is the solid angle in  $\mathbf{q}$  space) and  $R_{\alpha_1 \dots \alpha_l}^l(q)$  are Cartesian correlation moments given by

$$R_{\alpha_1 \dots \alpha_l}^l(q) = \frac{(2l+1)!!}{l!} \int \frac{d\Omega_{\mathbf{q}}}{4\pi} A_{\alpha_1 \dots \alpha_l}^l(\Omega_{\mathbf{q}}) R(\mathbf{q}). \quad (4)$$

Here, the coordinate axes are oriented so that  $z$  (long) is parallel to the beam direction,  $x$  (out) points in the direction of the total momentum of the pair in the LCMS frame and  $y$  (side) is chosen to form a right-handed coordinate system with  $x$  and  $z$ .

The correlation moments, for each order  $l$ , can be calculated from the measured 3D correlation function using Eq. (4). Alternatively, Eq. (2) can be truncated so as to include all non-vanishing moments and expressed in terms of independent moments only. As expected from symmetry considerations, moments odd in any coordinate were found to be consistent with zero within statistical uncertainty. Up to order  $l = 4$ , there are 6 independent moments:  $R^0$ ,  $R_{x^2}^2$ ,  $R_{y^2}^2$ ,  $R_{x^4}^4$ ,  $R_{y^4}^4$  and  $R_{x^2 y^2}^4$ , where  $R_{x^2}^2$  is shorthand for  $R_{xx}^2$ , etc. The independent moments can then be extracted as a function of  $q$  by fitting the truncated series to the experimental 3D correlation function with the moments as the parameters of the fit. The present analysis emphasizes the second method, with the moments computed up to order  $l = 4$  (higher order moments are found to be negligible). The moments are shown in Fig. 2, for the multipolarity orders of  $l = 2$  and 4, and in Fig. 1(a) for  $l = 0$  ( $1 + R^0(q) \equiv C^0(q)$ ).<sup>2</sup> The magnitude of the moment  $R_{x^2 y^2}^4$  is comparable to that of  $R_{x^4}^4$  and  $R_{y^4}^4$ .

Substitution of  $C(\mathbf{q})$  and  $S(\mathbf{r})$ , from Eq. (2) and Eq. (3), into the 3D form of the Koonin–Pratt equation

$$C(\mathbf{q}) - 1 = \int d\mathbf{r} K(\mathbf{q}, \mathbf{r}) S(\mathbf{r}) \quad (5)$$

results [13] in a relationship between corresponding correlation  $R_{\alpha_1 \dots \alpha_l}^l(q)$  and source moments  $S_{\alpha_1 \dots \alpha_l}^l(r)$ , which is similar to the 1D Koonin–Pratt equation:

$$R_{\alpha_1 \dots \alpha_l}^l(q) = 4\pi \int dr r^2 K_l(q, r) S_{\alpha_1 \dots \alpha_l}^l(r), \quad (6)$$

but now pertains to moments describing different ranks of angular anisotropy  $l$ . Since the mathematical structure of Eq. (6) is the

<sup>2</sup>  $C^0(q)$  agrees with 1D correlation function  $C(q)$  attesting to the reliability of the moment extraction technique.

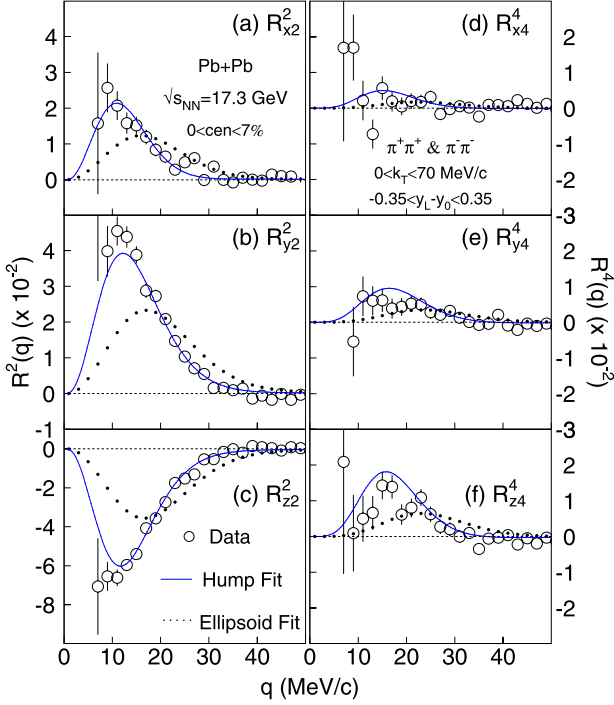


**Fig. 2.** (Color online.) Correlation moments for multipolarity  $l=2$  (left panels), and  $l=4$  (right panels) for mid-rapidity  $\pi^+\pi^+$  and  $\pi^-\pi^-$  pairs. Error bars indicate statistical errors only; systematic uncertainties are smaller than statistical ones.

same as that of Eq. (1), the same imaging technique can be used to invert the kernel  $K_l$  of the relation to extract the source moment  $S_{\alpha_1 \dots \alpha_l}^l(r)$  from the corresponding correlation moment  $R_{\alpha_1 \dots \alpha_l}^l(q)$ . Finally, the total 3D source function is calculated by combining the source moments for each  $l$  as in Eq. (3).

Alternatively, the source function can be extracted by directly fitting the 3D correlation function with an assumed 3D shape for the source function. Since the 3D correlation function can be represented by the Cartesian moments in the harmonic decomposition, the 3D fit corresponds to fitting the six independent non-trivial moments simultaneously with a trial source function.

Figs. 1–2 show the result of direct fits to the independent correlation moments with two 3D functions: (a) a single triaxial Gaussian, or ellipsoid, (dotted curve) and (b) a Hump shape (solid curve). As mentioned, the ellipsoidal fit, with four free parameters, fails to capture the low  $q$  behavior in  $C(q)$  and the large  $r$  behavior in  $S(r)$ . On the other hand, the Hump function, with six free parameters, gives a good fit. The form of the Hump function is

$$S(x, y, z) = \Lambda \exp \left[ -f_s \frac{r^2}{4r_s^2} - f_l \left( \frac{x^2}{4r_{xl}^2} + \frac{y^2}{4r_{yl}^2} + \frac{z^2}{4r_{zl}^2} \right) \right] \quad (7)$$

where  $r^2 = x^2 + y^2 + z^2$  and the coefficients  $f_s$  and  $f_l$  of the short and long-ranged components are given by  $f_s = 1/[1 + (r/r_0)^2]$  and  $f_l = 1 - f_s$  respectively. Here, the argument of the exponential shifts the behavior from that of a simple spherically symmetric Gaussian for  $r \ll r_0$  to that of a triaxial Gaussian for  $r \gg r_0$ . The parameter  $\Lambda$  regulates the fraction of pion pairs of which correlations are described in terms of the Hump function.<sup>3</sup>

<sup>3</sup> The fit parameters for the Hump are  $\Lambda = 0.281 \pm 0.006$ ,  $r_0 = 5.8 \pm 0.3$ ,  $r_s = 2.5 \pm 0.1$ ,  $r_{xl} = 6.9 \pm 0.1$ ,  $r_{yl} = 6.0 \pm 0.1$ ,  $r_{zl} = 10.9 \pm 0.3$ . Those for the ellipsoid (i.e.  $f_s \approx r_0 = 0$ ) are  $\Lambda = 0.198 \pm 0.003$ ,  $r_{xl} = 5.46 \pm 0.04$ ,  $r_{yl} = 4.95 \pm 0.04$ ,  $r_{zl} = 7.67 \pm 0.08$ .

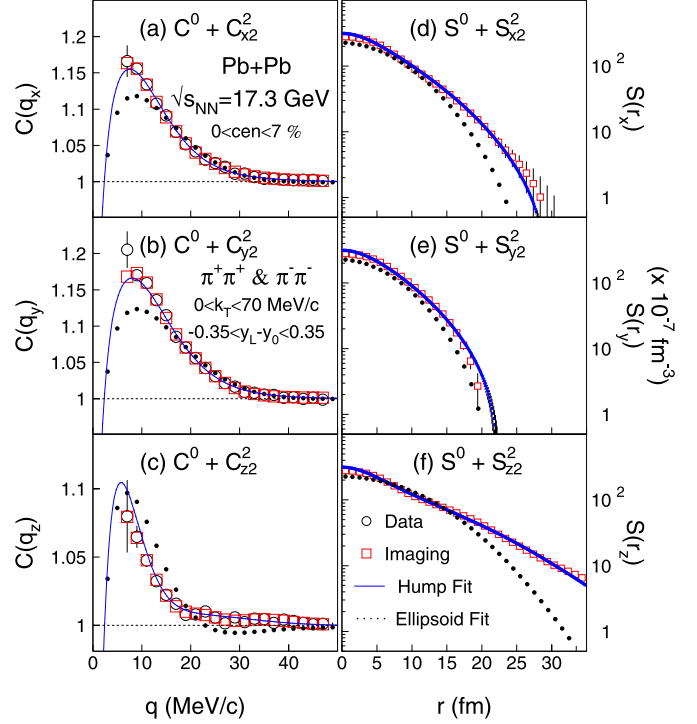


**Fig. 3.** (Color online.) Correlation  $C(q_i)$  (left panels) and source  $S(r_i)$  (right panels) function profiles for  $\pi^+\pi^+$  and  $\pi^-\pi^-$  pairs in the outward  $x$  (top panels), sideward  $y$  (middle) and longitudinal  $z$  (bottom) directions. The use of symbols is analogous to that in Fig. 1. Error bars indicate statistical errors only; systematic uncertainties are smaller than statistical ones. Here,  $l=4$  moments make negligible contributions.

Source imaging involves no assumptions on the analytical shape of the 3D source function. On the other hand, the moment fitting explicitly invokes a particular form for the 3D source function. The ellipsoid fit produces a  $\chi^2/ndf$  value of 6.8 while the Hump produces 1.2, which indicates a better fit to the observed correlation moments, as is visually evident in Figs. 1(a) and 2. Close agreement between the experimental data, the Hump fit and the restored correlation moments from imaging (see Figs. 1–2) strongly suggests that this assumed functional form properly represents the emission source. However, the uniqueness of the source function is, for example, not guaranteed beyond the region to which data are sensitive such as  $r > 40$  fm or where the source function is very small.

Figs. 3(d)–(f) show comparisons between two-pion source functions obtained via the fitting (lines) and the imaging (squares) techniques. The ellipsoid fit function (dotted line) underestimates the source image (squares) and Hump fit function (solid line) for  $r > 15$  fm in the  $x$  and  $z$  directions while the Hump fit function is in good agreement with the source image in the  $x$ ,  $y$  and  $z$  directions. This consistency check emphasizes the high degree of integrity with which the 3D source function is being extracted. The source function in the  $z$  direction is characterized by a long tail which extends beyond 30 fm. The source function in  $x$  also has a non-Gaussian tail, which, for this low  $p_T$  cut is less prominent than that in  $z$ . These aspects are decidedly different from those of a RHIC study [23].

The difference between the source functions from the ellipsoid fit and imaging procedures is also evident from a comparison of the corresponding correlation functions in the  $x$ ,  $y$  and  $z$  directions as shown in Fig. 3(a)–(c) respectively. Again there is consistency between the data, Hump fit and restored correlation functions in all three directions while the differences between the ellipsoid and

Hump fit sources for  $r \gtrsim 15$  fm are manifest by differences between the respective correlation functions for  $q \gtrsim 15$  MeV/c.

The event simulation code THERMINATOR allows for tests of the emission dynamics and of the breakup time of the reaction systems [24,18–20]. The code simulates thermal emissions from a cylinder with input transverse radius  $\rho_{\max}$ . Bjorken longitudinal boost invariance is assumed, and an expansion with transverse radial velocity  $v_r(\rho) = (\rho/\rho_{\max})/(\rho/\rho_{\max} + v_t)$ , where  $v_t = 1.41$ , in the Blast-Wave mode of the code. A fluid element ring, defined by  $\rho$  and  $z$ , breaks up at proper time  $\tau$  and lab frame time  $t$  where  $t^2 = \tau^2 + z^2$ . The freezeout hypersurface is specified by  $\tau = \tau_0 + a\rho$  where  $a$ , the space-time correlation parameter, is set to  $-0.5$  as was found in Ref. [20]. The negative value of  $a$  implies “outside-in” burning of the source i.e. outer particles are emitted earlier than inner ones, while a positive value of  $a$  would imply the reverse i.e. source emission from inside out. An emission duration parameter  $\Delta\tau$  is also needed to achieve a good fit. All known hadronic resonance decays are included.

THERMINATOR parameters  $v_t$ ,  $T$ ,  $\mu_B$ ,  $\mu_s$ ,  $\mu_i$  and  $a$  are taken from Refs. [18–20,25] as obtained from spectra and particle yields. Values of  $\rho_{\max}$ ,  $\tau_0$  and  $\Delta\tau$  were obtained by matching THERMINATOR’s generated source function to data shown in Figs. 3(d–f). The value of the transverse radius  $\rho_{\max}$  is chosen so as to reproduce the source function profile in the  $y$  direction;  $S(r_y)$  is insensitive to  $\tau_0$  and  $\Delta\tau$ . The proper lifetime  $\tau_0$  is determined by the short-range behavior of the source function profiles in the  $x$  and  $z$  directions. The proper emission duration is then determined by the tails of the source profiles in the  $x$  and  $z$  directions.

The calculation gives a good match to the experimental source function in the  $x$ ,  $y$  and  $z$  directions with a transverse dimension  $\rho_{\max} = 7.5 \pm 0.1$  fm, proper lifetime  $\tau_0$  ( $\tau = \tau_0$  at  $\rho = 0$ ) of  $7.3 \pm 0.1$  fm/c, a proper emission duration  $\Delta\tau = 3.7 \pm 0.1$  fm/c and  $a = -0.5$  (solid circles) [26]. The errors quoted are from the matching procedure alone. With these values of  $\rho_{\max}$ ,  $\tau_0$  and  $\Delta\tau$  we have reexamined the role of  $a = -0.5$  i.e. outside-in burning. Fig. 4 shows a comparison of the THERMINATOR source function, calculated using various values of  $a$  and other previously tuned parameters [25], with the extracted source function. The open symbols show that the calculations with  $a \geq 0$  overstate the extracted source function profile in the  $z$  direction. Attempts to compensate for this overshoot via different combinations of  $\rho_{\max}$ ,  $\tau_0$  and  $\Delta\tau$  were unsuccessful. Therefore, this failure suggests that a negative value for  $a$ , hence “outside-in” particle emission, is required to reproduce the extracted source function. The success of the THERMINATOR model simulation in precisely reproducing the experimental source function indicates consistency with approximate boost invariance at mid-rapidity, blast-wave dynamics for transverse flow, and outside-in burning in the evolution of the expanding system.

Results from this study and those from Ref. [7] depend on the different analysis techniques and models employed. The deduced time scales are similar but the geometric transverse radius is quite different. This difference results from the inclusion of resonances in THERMINATOR, as well as different parametrizations of  $T$  and  $v_r(\rho)$ . Conclusions from these THERMINATOR parameters are, of course, model dependent and therefore not necessarily unique. Different model assumptions may possibly lead to different pictures of the reaction dynamics [27].

In summary, we have presented a three-dimensional femto-scopic study of the two-pion source function in Pb + Pb collisions at  $\sqrt{s_{NN}} = 17.3$  GeV. A model-independent imaging/fitting technique reveals prominent non-Gaussian tails in the outward and longitudinal directions of the extracted source function. THERMINATOR Blast-Wave model calculations, incorporating Bjorken longitudinal flow, give a near-exponential tail in the longitudinal di-

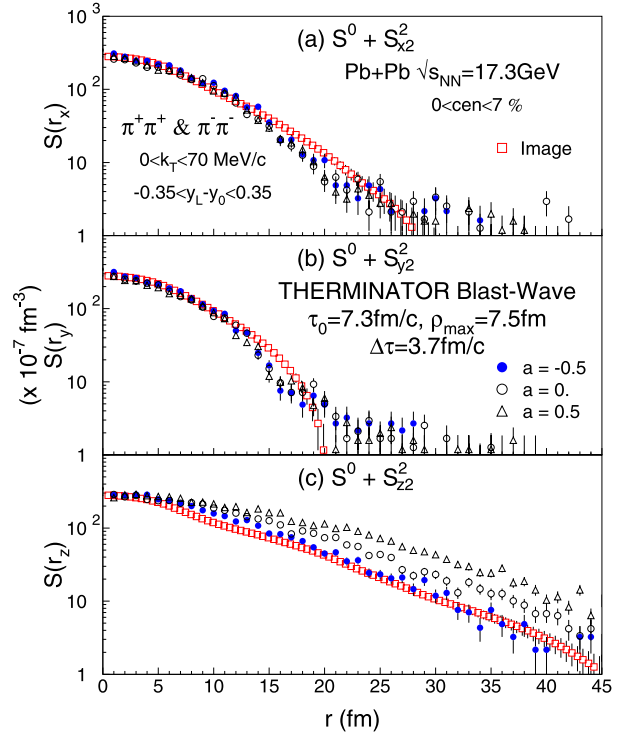


**Fig. 4.** (Color online.) Source function profiles,  $S(r_i)$ , comparison in the (a)  $x$ , (b)  $y$  and (c)  $z$  directions between the imaged data (squares) and THERMINATOR Blast-Wave model with various values of  $a$  (circles and triangles). Error bars indicate statistical errors only; systematic uncertainties are smaller than statistical ones.

rection consistent with observation. The space-time correlation parametrization suggests outside-in burning and provides values of the proper time for breakup and the emission duration.

## Acknowledgements

This work was supported by the US Department of Energy Grant DE-FG03-97ER41020/A000 and DE-FG02-03ER41259, the Bundesministerium für Bildung und Forschung, Germany, 06F 137, the Virtual Institute VI-146 of Helmholtz Gemeinschaft, Germany, the Polish State Committee for Scientific Research (1 P03B 006 30, 1 P03B 097 29, 1 P03B 121 29, 1 P03B 127 30), the Hungarian Scientific Research Foundation (T032648, T032293, T043514), the Hungarian National Science Foundation, OTKA (F034707), the Polish-German Foundation, the Korea Science & Engineering Foundation (R01-2005-000-10334-0), the Bulgarian National Science Fund (Ph-09/05), the Croatian Ministry of Science, Education and Sport (Project 098-0982887-2878), the National Science Foundation NSF PHY-0555893 and PHY-0800026.

## References

- [1] E.V. Shuryak, Nucl. Phys. A 750 (2005) 64.
- [2] S. Pratt, Phys. Rev. Lett. 53 (1984) 1219;  
K. Kolehmainen, M. Gyulassy, Nucl. Phys. A 461 (1987) 239c;  
K. Kolehmainen, M. Gyulassy, Phys. Lett. B 180 (1986) 203;  
A. Makhlin, Y. Sinyukov, Z. Phys. C 39 (1988) 69.
- [3] K. Adcox, et al., Nucl. Phys. A 757 (2005) 184.
- [4] G. Goldhaber, et al., Phys. Rev. 120 (1960) 300;  
G.I. Kopylov, M.I. Podgoretsky, Sov. J. Nucl. Phys. 15 (1972) 219;  
G. Cocconi, Phys. Lett. B 49 (1974) 459;  
M. Lisa, et al., Annu. Rev. Nucl. Part. Sci. 55 (2005) 357.
- [5] S. Chapman, J.R. Nix, Phys. Rev. C 54 (1996) 866.
- [6] H. Appelshäuser, et al., Eur. Phys. J. C 2 (1998) 661.
- [7] C. Alt, et al., Phys. Rev. C 77 (2008) 064908.
- [8] D. Brown, P. Danielewicz, Phys. Lett. B 398 (1997) 252.

- [9] D. Brown, P. Danielewicz, Phys. Rev. C 57 (1998) 2474.
- [10] D. Brown, P. Danielewicz, Phys. Rev. C 64 (2001) 14902.
- [11] P. Chung, et al., Nucl. Phys. A 749 (2005) 275c.
- [12] S. Adler, et al., Phys. Rev. Lett. 98 (2007) 132301.
- [13] P. Danielewicz, S. Pratt, Phys. Lett. B 618 (2005) 60.
- [14] D.A. Brown, et al., Phys. Rev. C 72 (2005) 054902.
- [15] P. Danielewicz, S. Pratt, nucl-th/0612076v2, 2007.
- [16] P. Chung, et al., Nucl. Phys. A 774 (2005) 919.
- [17] S. Afanasiev, et al., Phys. Rev. Lett. 100 (2008) 232301.
- [18] A. Kisiel, et al., Comput. Phys. Commun. 174 (2006) 669.
- [19] A. Kisiel, Brazilian J. Phys. 37 (3A) (2007) 917.
- [20] A. Kisiel, et al., Phys. Rev. C 73 (2006) 064902.
- [21] S. Afanasiev, et al., Nucl. Instrum. Methods A 430 (1999) 210.
- [22] R. Lednicky, et al., Phys. Part. Nucl. 35 (2004) S50.
- [23] P. Chung, et al., J. Phys. G: Nucl. Part. Phys. 34 (2007) 1.
- [24] P. Chung, P. Danielewicz, arXiv:0807.4892v1 [nucl-ex], 30 July 2008.
- [25] W. Broniowski, W. Florkowski, arXiv:hep-ph/0202059v1, 7 February 2002; M. Michalec, Ph.D. Thesis, nucl-th/0112044.  
Values used are:  $T = 164$  MeV for temperature,  $\mu_B = 229$  MeV,  $\mu_S = 54$  MeV,  $\mu_I = -7$  MeV for baryon, strangeness and isospin chemical potentials.
- [26] For this parameter set, THERMINATOR produces  $m_T$  spectra which are in very good quantitative agreement with the measurements reported in S.V. Afanasiev, et al., Phys. Rev. C 66 (2002) 054902.
- [27] M.A. Lisa, S. Pratt, arXiv:0811.1352 [nucl-ex].